# Electrochemistry in Hollow-Channel Paper Analytical Devices

Christophe Renault, Morgan J. Anderson, and Richard M. Crooks*

Department of Chemistry, Center for Nano- and Molecular Science and Technology, The University of Texas at Austin, 105 East 24th Street Stop A5300, Austin, Texas 78712-1224, United States

S *Supporting Information*

ABSTRACT: In the present article we provide a detailed analysis of fundamental electrochemical processes in a new class of paper-based analytical devices (PADs) having hollow channels (HCs). Voltammetry and amperometry were applied under flow and no flow conditions yielding reproducible electrochemical signals that can be described by classical electrochemical theory as well as finite-element simulations. The results shown here provide new and quantitative insights into the flow within HC-PADs. The interesting new result is that despite their remarkable simplicity these HC-PADs exhibit electrochemical and hydrodynamic behavior similar to that of traditional microelectrochemical devices.
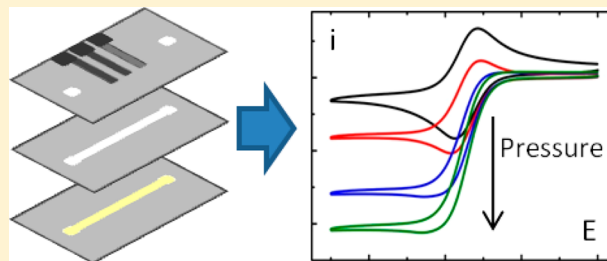
INTRODUCTION

In the present article we provide a detailed analysis of fundamental electrochemical processes in a new class of paper-based analytical devices (PADs) having hollow channels (HC-PADs). The interesting new result is that despite their remarkable simplicity these paper devices exhibit electrochemical behavior similar to that of traditional glass and plastic microfluidic electrochemical devices, in both the absence and presence of flow. This finding opens up new possibilities for electrochemical processing and detection in PADs. Moreover, because electrochemistry is likely the best detection method for quantitative, low limit-of-detection (LOD), point-of-care (POC) PADs,[1] the results reported here provide an important foundation on which to build future applications of this emerging technology.

The original reports of two-dimensional (2D) and three-dimensional (3D) PADs by the Whitesides group[2,3] in 2007 and 2008, respectively, stimulated research in the field of highly functional paper-based sensors.[4−15] This is a consequence of the fact that the characteristics of this family of devices are well-matched to the needs of the POC diagnostic community. The relevant properties include low cost, high surface-to-volume ratio, biocompatibility, ease of disposal, flexibility, and ability to carry out rapid prototyping.

The original 3D PADs were fabricated by patterning individual sheets of paper and then taping them together.[3] Subsequently, we took advantage of the flexibility of paper to simplify multidimensional fabrication by folding the paper into desired configurations.[16] We call such fluidic devices origami PADs or oPADs. In addition to flexibility, another important property of paper is that water spontaneously flows through it by capillary action, thereby avoiding the need for pumping equipment.[12] Most PADs rely on capillary flow to both direct and time the flow of analytes.[17−20] While capillary-driven flow is advantageous in many regards, the presence of the cellulose

matrix introduces several difficulties such as low rates of convective mass transfer, significant nonspecific adsorption due to the high surface area of the cellulose fibers, and a size restriction on the mobility of objects within the cellulose matrix due to the size-exclusion properties of paper.

One approach for relieving some of the shortcomings inherent to the paper format is to simply remove the cellulose matrix from within the channel and introduce analytes directly into the void space of the resulting HC. Thus far, there are just two reports of HC paper fluidic devices. In the first of these, Glavan et al. engraved a trench in thick cardstock paper, rendered it omniphobic by gas-phase infusion of a fluoroalkyl silane, and then sealed the top of the trench with tape.[21] The resulting HCs were too hydrophobic to allow capillary flow, so fluids were pushed through the channels using a syringe pump. In this configuration, fast, laminar flow was achieved. However, because of the pumping requirement, these HCs are not appropriate for most POC applications. The second example of HC paper-based devices comes from our group.[22] In this case, the channels are constructed by wax patterning a sheet of chromatographic paper, cutting out the channel, and then folding the paper into the final device configuration. A small portion of exposed (not coated with wax) cellulose is left on the floor of these devices, and consequently the channels are sufficiently hydrophilic that a single drop of liquid (corresponding to a pressure of ∼0.2 mbar) is sufficient to induce fast pressure-driven flow. We demonstrated that such devices are applicable for POC applications by fabricating a simple HC-PAD for colorimetric detection of glucose and bovine serum albumin. We also showed that obstacles present in the HCs, such as paper barriers and hydrophobic weirs, can be used to slow, or even stop, fluid flow. Having shown that we can

control the flow in these devices, as well as perform basic colorimetric assays, we aim to implement analytical techniques with lower LODs and higher sensitivity.

As stated previously, electrochemical detection is very well matched to paper-based POC assays that require a quantitative readout, low LODs, and low cost of instrumentation. Indeed, a number of electrochemical strategies developed for bulk solution sensors have been adapted to paper platforms following the Henry group's first report of electrochemical detection in PADs.[23] These include amperometric and potentiometric detection of glucose,[23,24] lactate,[23,25] uric acid,[23,26] ascorbic acid,[26] β-D-galactosidase,[27] cholesterol,[25] Pb^{2+},[24] H$_2$O$_2$,[28] and cancer markers.[29] In all of these cases the electrodes were in direct contact with paper.

In the present article we show that removal of the cellulose fibers from the channels results in rapid mass transfer. The flow rate within the channel was quantified by electrochemical methods for pressures ranging from 0.3 to 4.5 mbar. Voltammetry and amperometry were applied under flow and no-flow conditions and yielded reproducible signals that can be described by classical electrochemical theory as well as finite-element simulations. The results shown here provide new and highly quantitative insights into the mass transfer and electrochemical properties of HC-PADs.

■ EXPERIMENTAL SECTION

Chemicals and Materials. Ferrocenemethanol (FcMeOH) and 1,1'-ferrocenedimethanol (FcDM) were purchased from Sigma-Aldrich (St. Louis, MO). Whatman grade 1 chromatography paper (20 cm ×20 cm sheets), NaCl, and concentrated pH 7.4 phosphate buffered saline solution (PBS 10X, 119 mM phosphate, 1.37 M NaCl, and 27 mM KCl) were purchased from Fisher Scientific (Waltham, MA). Tris(1,10-phenanthroline) iron(II) sulfate (Fe(phen)$_3$SO$_4$) and resazurin were purchased from Acros Organics (Morris Plains, NJ). Tartrazine was purchased from MP Biomedicals LLC (Solon, OH). 4′,6-Diamidino-2-phenylindole, dihydrochloride (DAPI) was purchased from Life Technologies (Carlsbad, CA). The carbon (CI-2042) and Ag(83%)/AgCl(17%) (CI-4002) inks were purchased from Engineered Conductive Materials (Delaware, OH). The solutions were prepared using deionized water (18.2 MΩ·cm, Milli-Q Gradient System, Millipore). All chemicals were used as received.

Device Fabrication. The HC-PADs were fabricated using a previously reported wax patterning method.[22] The patterns were designed using CorelDraw12 software and printed on Whatman grade 1 chromatographic paper using a Xerox 8570DN inkjet wax printer. The patterns used for the different paper devices are provided in the Supporting Information (Figure S1). After printing, the paper was placed in an oven at 125 °C for 1 min to melt the wax, and then it was cooled to 23 °C. The carbon and Ag/AgCl electrodes were screen-printed directly on the paper devices using a mesh with 305 threads per inch^2 (Ryonet Corporation, Vancouver, WA). The inks were then cured in an oven at 65 °C for 30 min. Channels and reservoirs larger than 2 mm were cut using a razor blade and a 4-mm-diameter punch (Harris Unicore), while smaller HCs were cut using a laser cutter (Epilog Zing 16 from Epilog Laser, Golden, CO. Parameters: Vector image, Speed: 90%, Power: 10%, Frequency: 1500 Hz). In all cases, clean cuts are required to avoid clogging the channels. After cutting the channels, the paper was folded into the final device configuration (Scheme 1), sandwiched between two rigid, 5 mm-thick poly(methyl methacrylate) holders, and then clamped with binder clips. Copper tape (3M) was used to establish contact between the screen-printed electrodes and the potentiostat.

Electrochemical Measurements. Electrochemical measurements were carried out at room temperature (23 ± 1 °C) using a potentiostat (650 C, CH Instruments, Austin, TX) or bipotentiostat (700 E, CH Instruments, Austin, TX). In some cases a Pt wire counter electrode and a reference electrode (either a glass Ag/AgCl, 1 M KCl or a

Scheme 1

Scheme 1

3D view

Top

fold

fold

wax □ void
■ electrode
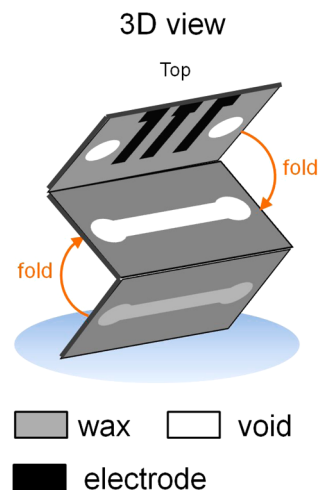
saturated calomel electrode (SCE), CH Instruments, Austin, TX) were placed into the outlet reservoir of the HC-PAD. The ohmic resistance in the HCs was electronically compensated (R_{comp}). At the end of each experiment, the paper devices were opened and visually inspected. No changes, such as formation of holes or delamination, were observed even after prolonged periods of flow. We also explored (results not shown) a large potential window (from roughly ±1 V vs Ag/AgCl, 1 M KCl) and did not observe a change in the electrochemical properties of the carbon screen-printed electrodes.

Numerical Simulations. Numerical simulations were performed using a Dell Precision T7500 Simulation workstation outfitted with Dual Six Core Intel Xeon Processors (2.40 GHz) and 24 GB of RAM. Simulations were carried out using the COMSOL Multiphysics v4.3 commercial package. All simulations were performed in 2D. Convective models solved the Navier−Stokes equation, assuming an incompressible fluid and no-slip boundary conditions on the floor and ceiling. Convection−diffusion simulations were performed assuming that the concentration of analyte was zero at the electrode surface, corresponding to the mass-transfer-limited case. A full discussion of the simulations is provided in the Supporting Information.

■ RESULTS AND DISCUSSION

Electrochemistry in Absence of Convection. Scheme 1 shows a 3D view of an HC-PAD before assembly. Cross-sectional micrographs of the folded device are provided in Figure S2, and the thickness of the different layers is given in Table S1. Briefly, the cell consists of three wax-patterned paper layers having a thickness of 170 ± 10 μm. A channel cut from the middle paper layer defines the HC, which is 2 mm wide (w), 170 μm high (h), and 30 mm long. The bottom-most layer is partially waxed, so that the bottom of the device is wax but the floor of the channel is unwaxed (and hence hydrophilic) to a depth of 70 ± 10 μm (light gray color in Scheme 1). A complete description of the thickness of each layer is provided in Table S1 in the Supporting Information. Cross-sectional micrographs of dry and wet HCs are compared in Figure S3. These micrographs show that, in presence of water, the height of the channel is reduced. Thus, the measured dimensions of dry HC-PADs only provide an estimate of the HC size and do not accurately reflect the *operando* dimensions. In some cases (4 out of 15 devices) we observed an abnormally low flow rate in the HC-PAD which we attribute to significant distortions of the channel geometry as observed in Figure S3d and S3f. The roughness and contact angle of water for each layer are provided in the Supporting Information (Table S2). As
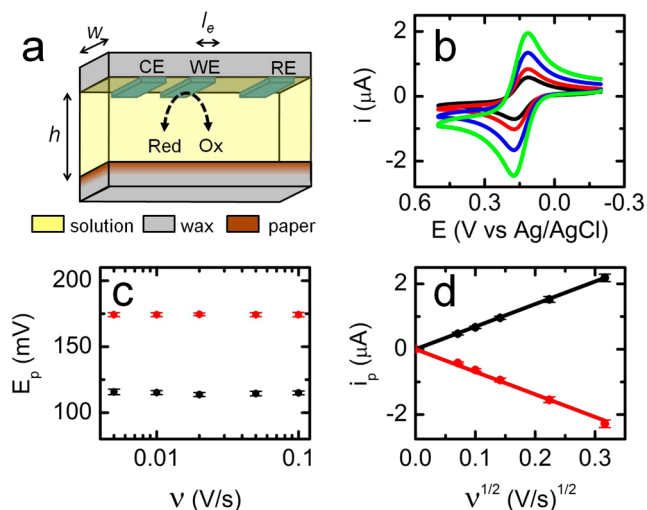
Figure 1. (a) A 3D schematic illustration of a three-electrode HC paper electrochemical cell. The scheme is not drawn to scale. A detailed description of the cross section is provided in Figure S2 and Table S1. (b) CVs recorded using an HC-PAD like the one presented in (a). The channel was filled with a solution containing 250 μM FcMeOH and PBS 1X. The black, red, blue, and green lines correspond to ν = 10, 20, 50, and 100 mV/s, respectively. The solution was not flowing during the experiments. R_{comp} = 7 kΩ and the geometric area of the WE (S_{WE}) was 0.040 ± 0.004 cm^2. (c) Variation of the anodic (red) and cathodic (black) peak-current potentials with ν. (d) The anodic (red) and cathodic (black) peak currents as a function of $\nu^{1/2}$. In (c) and (d) the error bars represent the standard deviations observed using three independent devices.

discussed in our previous report,[22] the hydrophilic floor of the HC plays a crucial enabling role, in that it enables fluid flow at very low pressures. The configuration of the HC electrochemical cell is illustrated in Figure 1a. The working, counter, and reference electrodes (WE, CE, and RE, respectively) are screen-printed directly on the ceiling of the HC (Figure 1a). For these experiments, the WE and CE are made with a carbon paste while the reference is made with a Ag/AgCl paste. These electrodes are 2 mm long (l_e) and span the entire width of the channel. Note that the placement of the electrodes on the ceiling is important, because when they are present on the paper floor they represent hydrophobic barriers that can stop fluid flow at low pressures.

The first part of this study focuses on HC electrochemistry in the absence of convection. The electrochemical behavior of the HC-PADs was characterized by cyclic voltammetry (CV) using FcMeOH as a redox probe. These experiments were carried out by flowing a solution containing 250 μM FcMeOH and PBS 1X through the HC for 5 min, stopping the flow, and then recording CVs at scan rates (ν) between 10 and 100 mV/s (Figure 1b). The resulting anodic and cathodic peak potentials (E_p) are plotted as a function of ν in Figure 1c, and the anodic and cathodic peak currents (i_p) are plotted as a function of $\nu^{1/2}$ in Figure 1d. The straight lines in Figure 1d are values of i_p calculated using the Randles−Sevcik equation (details are provided in the Supporting Information). The error bars in both plots correspond to standard deviations for measurements obtained from three independently prepared HC-PADs. The coefficients of variation, defined as the standard deviation divided by the average, are 2% and 10% for E_p and i_p, respectively, indicating good device-to-device reproducibility.

This point is of critical importance for quantitative sensing applications.

The shape of the CVs in Figure 1b, the peak separations of 59 ± 3 mV observed in Figure 1c, and the linear variation of i_p with $\nu^{1/2}$ are characteristic of a reversible electrochemical system acting under one-dimensional (1D) semi-infinite diffusion.[30] Because the diffusion coefficients of the reduced and oxidized forms of FcMeOH are nearly the same ($D_{ox} = D_{red}$ = 6.7 × 10^{-6} cm^2/s),[31] the formal potential, $E^{\circ\prime}$, is equal to the average of the peak potentials: 145 mV vs Ag/AgCl.[30] This value is close to the literature value of 150 mV vs Ag/AgCl.[32] We also observed that the potential of the screen-printed Ag/AgCl reference electrode is stable for at least 30 min, which is also the approximate lifetime of an HC-PAD. Taken together, the results in Figure 1 demonstrate good agreement with expectations from classical electrochemistry. This means that nonidealities of the system, which include the roughness and wetability of the wax and paper channels walls, conductivity of the electrodes,[33,34] and the constrained channel geometry, do not substantially affect the performance or reproducibility of HC-PADs over the range of experimental variables considered here.

In addition to cyclic voltammetry we also performed chronoamperometry (CA) using the HC-PAD shown schematically in Figure 1a. Current, corresponding to the mass-transfer-limited oxidation of FcMeOH, is plotted as a function of $t^{1/2}$ in Figure 2a (black line) for times between 2 and 60 s.[30] CAs measured at longer times are provided in Figure S4. The blue line in Figure 2a is a plot of the Cottrell equation for this system (details are provided in the Supporting Information). At short times (<15 s), a linear relationship between i and $t^{-1/2}$ is observed for the experimental CA. This relationship is in agreement with the Cottrell equation, which describes the mass-transfer-limited current under the 1D semi-infinite boundary condition.[30] After ~15 s the magnitude of the current decreases faster than predicted by the Cottrell equation (inset in Figure 2a), resulting in a noticeable deviation from ideality. The magnitude of the deviation at 45 s is 30 ± 10 nA (measured using three independent devices).

To gain additional insight into the unusual behavior of the CA at t > ~15 s, a numerical simulation of the CA experiment was obtained. For the simulation, the paper floor was modeled as an organized porous layer in which FcMeOH freely diffuses in the pores, but not through the solid cellulose fibers. While the paper matrix is structurally complex, the simplification used here suffices for the level of detail we seek. More information about the simulation, particularly the treatment of diffusion in the cellulose floor, is provided in the Supporting Information.

The red line in Figure 2b is the simulated CA. The blue line is a linear extrapolation of the portion of the simulated CA between 2 and 7 s, and is provided only to emphasize the deviation from Cottrell behavior at longer times. Between 2 and 15 s, the simulated current varies linearly with $t^{1/2}$. However, after 15 s the magnitude of the simulated current decreases faster than would be expected based on Cottrell behavior (blue line). These observations are in qualitative agreement with the experimental data shown in Figure 2a, but it should be noted that a quantitative discrepancy exists between the simulation and the experiment. At 45 s the deviation between the simulated CA and the Cottrell (blue) line (~90 nA) is three times larger than the experimental deviation (30 ± 10 nA). Possible causes of the discrepancy could be nonidealities associated with the low currents and long time scale of the
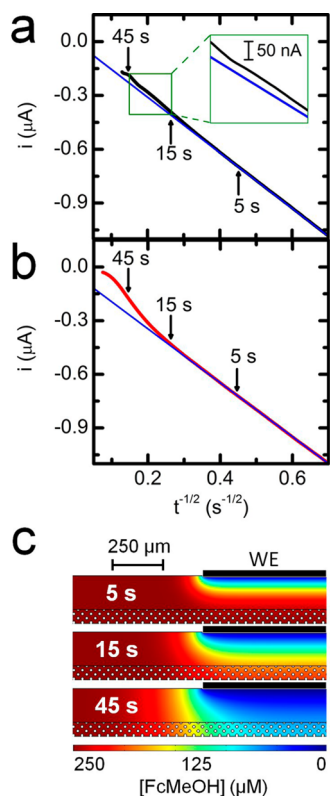
Figure 2. (a) The black line is an experimentally determined CA corresponding to the oxidation of FcMeOH in an HC-PAD similar to that shown in Figure 1a. The potential was stepped from −0.100 V to +0.400 V vs Ag/AgCl, [FcMeOH] = 250 μM (in PBS 1X), and S_{WE} = 0.040 ± 0.004 cm^2. In that particular experiment the ohmic resistance was not compensated. The blue line is a plot of the Cottrell equation (see Supporting Information). (b) The red line is a numerical simulation of the experiment represented in Figure 2a. Details regarding the simulation are provided in the text and in the Supporting Information. The blue line is an extrapolation of the linear part (2 to 7 s) of the simulated CA. (c) Concentration profiles of FcMeOH derived from the simulated CAs at 5, 15, and 45 s. The position of the WE in the channel is indicated by the thick black line. The white dots represent the cellulose fibers in the paper floor.

experiments (see Figure S4 and discussion in the Supporting Information).

Figure 2c shows three concentration profiles, corresponding to the three times (5, 15, and 45 s) indicated in Figure 2, obtained from the finite element simulation. These snapshots show that at 5 s the diffusion layer thickness is still smaller than the height of the channel, and thus diffusion of FcMeOH can be considered as semi-infinite. At ~15 s the edge of the diffusion layer (indicated by a light red color) completely penetrates the paper floor (indicated by the white dots). This corresponds to the onset of deviation from 1D semi-infinite diffusion observed in Figure 2b. After 45 s, the diffusion layer has expanded further into the floor of the HC, significantly depleting the concentration of FcMeOH directly below the electrode (indicated by the thick black line labeled WE). Clearly, the constraint of the diffusion layer by the floor of the channel explains the decrease in current observed in the CAs at t > 15 s.

For poly(dimethylsiloxane) (PDMS) microchannels, it has previously been shown that constraint of the diffusion layer can dramatically affect the electrochemical response yielding, in

extreme cases, a "thin layer" mass transfer regime.[35] Under the experimental conditions used here the current does not drop to zero as expected for an ideal thin layer electrochemical cell.[30] The primary reason for this observation is that the diffusion layer continues to extend axially along the channel length (Figure 2c). However, the important result is that under no-flow conditions most of the volume of the HC below the electrode is probed by diffusion after only 15 to 45 s.

Laminar Flow. In this section we discuss the nature of the flow regime within the channels of the HC-PADs. To carry out these experiments, we first used the HC-PAD design illustrated schematically in Figure 3a. This device consists of a "Y" shaped
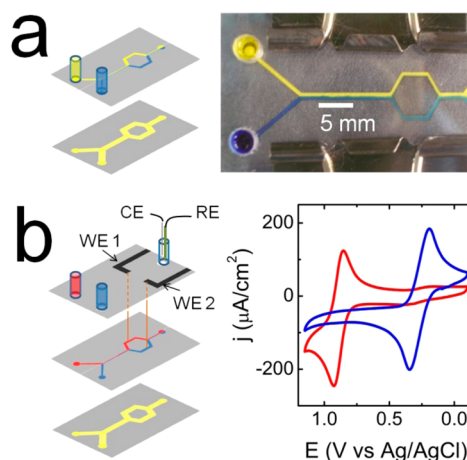

Figure 3. (a) Schematic illustration and photograph demonstrating qualitatively that a laminar flow is obtained in HC-PADs. Two aqueous solutions containing 1.0 mM tartrazine (yellow) or 50.0 mM resazurin (blue) were introduced at the two inlets. (b) Schematic illustration of the HC-PAD used to quantify the laminar flow. Note that the two WEs partially cross the HCs. The CE and RE were, respectively, a Pt wire and a glass Ag/AgCl, 1 M KCl electrode placed in the outlet reservoir. The red and blue reservoirs were filled with a saline solution (0.5 M NaCl) containing 1.0 mM Fe(phen)SO$_4$ and 1.0 mM FcDM, respectively. The solutions were allowed to flow for 2 min, and then the flow was stopped immediately prior to recording the CVs. ν = 100 mV/s; R_{comp} = 6 kΩ; S_{WE1} = 0.029 cm^2; S_{WE2} = 0.021 cm^2.

inlet that merges into a single main channel. Toward the center of the main channel, the stream is split again into two separate channels. If the flow is laminar, then the solutions are expected to mix only by diffusion. Given the short time of contact between the two coflowing streams (<10 s) and the width of the streams (1 mm), mixing by diffusion is negligible.[36,37] In contrast, a turbulent flow leads to fast mixing, which is readily detectable visually or by electrochemistry.[37]

Observation of the interior of the channel through the transparent plastic holder (see photograph in Figure 3a and note that the top paper layer was removed for these measurements) shows that two dye solutions having different colors do not mix while flowing in the main channel. That is, after the two colored solutions are directed into the same main channel and subsequently separated, there is no visual evidence of mixing. This result suggests that fluid flow is laminar even in these very crude HCs.

To confirm and quantify this result in the presence of the top wax layer supporting the electrodes (Figure 3b), electro-chemistry was used to monitor the composition of the solution in the device. In the design shown in Figure 3b, one WE is

placed within each of the two separated streams so that the composition of each can be independently analyzed. For that experiment, the CE (Pt wire) and RE (glass Ag/AgCl, 1 M KCl) were placed in the outlet reservoir. Two 0.5 M NaCl solutions, one containing 1.0 mM FcDM and the other 1.0 mM Fe(phen)$_3$SO$_4$ ($E^{\circ\prime}$ = 0.268 V vs Ag/AgCl, 1 M KCl and 0.890 V vs Ag/AgCl, 1 M KCl), respectively, as determined by voltammetry), were introduced into the two inlets.

The CVs shown in Figure 3b were obtained in the two separate branches of the HC after the flow stopped. The key result is that only FcDM is detected in the blue channel while mainly Fe(phen)$_3$SO$_4$ is observed in the red channel. Note, however, that a trace of FcDM is present in the red channel, which might be because of slightly unequal heights of the solutions at the inlets and hence different fluid velocities. Similar effects have been observed by Osborn et al. in paper devices.[18] These results indicate that the solutions of FcDM and Fe(phen)$_3$SO$_4$ do not mix significantly while flowing in the main channel, and therefore we conclude that under our experimental conditions the flow in HC-PADs is laminar. The experimental observation of laminar flow is further confirmed by the Reynolds number, R_e, which is always <5 in our experiments (calculation provided in the Supporting Information). The significance of the results described in this subsection is that because the laminar flow regime is well understood and allows for relatively straightforward theoretical analysis using numerical simulations, or in some cases analytical solutions,[38] it will be possible to use these simple HC-PADs to quantitatively interpret the outcome of electrochemical diagnostic assays in the future.

Determination of Flow Rate. To complete the characterization of flow in HC-PADs, we investigated the relationship between the flow rate and the pressure drop within the HC. The pressure drop (P) was controlled by adjusting the height difference (ΔH) between the columns of liquid in the inlet and outlet reservoirs (Figure 4a). The value of P was calculated using eq 1.

$$P = \rho \times g \times \Delta H \qquad (1)$$

Here, ρ is the density of water at 25 °C (997 kg/m^3) and g is the gravitational constant (6.674 × 10^{-11} m^3/(kg s^2)). Note that there was some variation in ΔH during the course of each experiment because of liquid transferring from the inlet to the outlet, but this differential was maintained below 10% to ensure a nearly constant flow rate.

The average linear flow rate (u_{av}) was measured by electrochemistry using the generation–collection experiment depicted in Figure 4a. A similar configuration was previously used by Wrighton and co-workers in a static (nonflowing) system[39] and later by Amatore and co-workers, who measured the flow rate in PDMS-based microchannels.[40] In our experiment, two WEs having a fixed edge-to-edge separation of l_{G-C} = 11.5 mm (Figure 4a) were defined in the HC, while the CE (Pt wire) and RE (SCE) were positioned in the outlet reservoir. The generation–collection experiment is initiated by stepping the potential of the generator electrode from −0.200 to 0.600 V vs SCE under flowing conditions. This results in oxidation of FcMeOH to FcMeOH$^+$. The latter then flows downstream to the collector electrode, which is held at a constant reducing potential of −0.200 V vs SCE to reduce FcMeOH$^+$ back to FcMeOH. Typical CAs for the generator and collector electrodes are shown in Figure 4b. The reduction of the FcMeOH$^+$ at the collector electrode gives rise to a
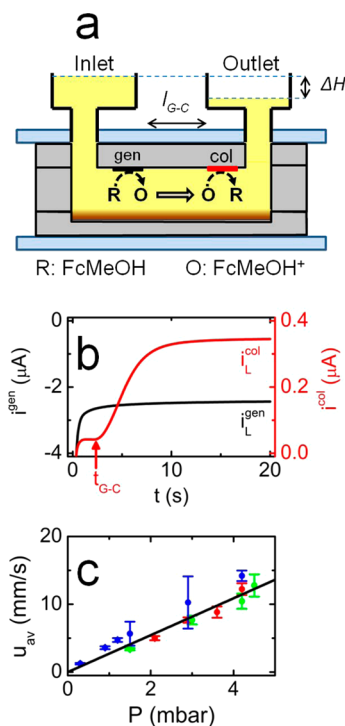

Figure 4. (a) A schematic illustration showing the HC electrochemical PAD used for generation-collection experiments. The color scheme is the same as in Scheme 1 and Figure 1a. The blue color represents the plastic holder of the device. The scheme is not drawn to scale. (b) Currents measured at the generator (black line) and collector (red line) electrodes during the CA experiment. The potential was stepped from −0.200 V vs SCE to 0.600 V vs SCE; $S_{gen} = S_{col}$ = 0.2 cm ×0.2 cm (0.04 cm^2); [FcMeOH] = 250 μM (in PBS 1X). The CE and RE were, respectively, a Pt wire and an SCE placed in the outlet reservoir. Each time the pressure was modified, the solution was allowed to flow for at least 5 min to ensure limiting behavior. The red arrow indicates the time delay, t_{G-C}, between the generation and the collection of FcMeOH$^+$. (c) Average linear flow rate (u_{av}) measured for the generation−collection experiment. The green, red, and blue circles correspond to measurements obtained using three independent devices. The error bars correspond to the standard deviation of at least 10 replicate measurements of t_{G-C}. The black line is a least-squares fit to the data (slope = 2.7 ± 0.2 mm/(s mbar); R^2 = 0.956).

sudden increase of cathodic current at $t = t_{G-C}$, indicated by the red arrow in Figure 4b. After a specified period of time, the currents at the generator and collector electrodes approach limiting values corresponding to i_L^{gen} and i_L^{col}, respectively.

The time delay, $t = t_{G-C}$, between the initial oxidation of FcMeOH at the generator electrode and the initial reduction of FcMeOH$^+$ at the collector electrode corresponds to the time necessary for the FcMeOH$^+$ to travel the distance l_{G-C}. The relationship between t_{G-C} and u_{av} is given by eq 2.[40]

$$u_{av} = \gamma \times \frac{l_{G-C}}{t_{G-C}} \qquad (2)$$

Here, γ is a dimensionless geometrical factor, which is assumed to be close to unity.[40] Values of t_{G-C} were measured for independently fabricated HC-PADs at different pressures (Table S2), and then t_{G-C} was converted into u_{av} using eq 2 (γ = 1; l_{G-C} = 11.5 mm). The values of u_{av} are plotted as a function of pressure in Figure 4c. As reported previously for plastic microfluidic devices,[38] u_{av} varies linearly with pressure. The slope of the best least-squares fit to the experimental data

(black line in Figure 4c) is 2.7 ± 0.2 mm/(s mbar). The coefficient of variation of u_{av} within a single device is 11% and from device to device 17%. This is relatively good considering the complexity of a generation−collection experiment and the inherent device-to-device variability of the paper platform.

To compare the flow rate in HC-PADs with that in traditional PADs, a generation−collection experiment was performed using a device identical to the HC-PAD, except that the cellulose fibers were left in the channel (details are provided in the Supporting Information). The variation of u_{av} with P in the paper-channel PAD was found to be only 0.0056 ± 0.0002 mm/(s mbar), or 480 times smaller than that in HC-PADs. This result simply illustrates that pressure-driven flow through a channel obstructed by cellulose fibers is much slower than that through an HC.

This foregoing result is important for understanding the solution flow profile within HCs. By analogy to electric currents flowing through two unequal resistances connected in parallel, the fluid flows primarily in the void part of the channel (section of lower hydraulic resistance), while only a small fraction flows within the hydrophilic floor which is partially obstructed by the cellulose fibers. In other words, u_{av} is much larger in the HC than in the paper floor, and hence flow within the cellulose matrix is negligible.

The experimentally determined values of i_L^{gen} and i_L^{col} (Figure 4b) were used to calculate the collection efficiency (N, eq 3) of the HC-PADs.

$$N = -\frac{i_L^{col}}{i_L^{gen}} \tag{3}$$

Under our experimental conditions, N varies between 0.1 and 0.3 for pressures ranging from 0.3 to 4.5 mbar, respectively (values of N measured for several pressures and devices are provided in Figure S5). Importantly, the measured values of N in the HC-PADs are comparable to values observed in glass and plastic microfluidic devices.[40,41]

The volumetric flow rate (Q) in HC-PADs was also measured by monitoring the variation of the liquid height in the outlet reservoir as a function of time (details concerning the experimental setup are provided in the Supporting Information, Figure S7). By comparing the volumetric flow rate and the linear flow rate determined by electrochemistry, the average cross-sectional area of the HC was determined to be 0.19 ± 0.03 mm^2 (details concerning the calculation are provided in the Supporting Information). This value is 44 ± 9% smaller than the value measured using cross-sectional micrographs of dry HCs (Table S1). The various nonidealities of the paper platform, such as structural deformation (Figure S3), roughness (Table S2), and degree of hydrophilicity (Table S2), are likely contributors to this observation.

Electrochemistry in the Presence of Convection. The reproducibility and predictability of flow rates within HCs are ideal for coupling convection to electrochemical detection. In this subsection, the effect of the flow rate on the current is qualitatively and quantitatively analyzed using convection−diffusion theories and numerical simulations.

An HC-PAD similar to the one presented in Figure 1a, that is with the WE (carbon paste), CE (carbon paste), and RE (Ag/AgCl paste) placed directly in the HC, was used to carry out the experiments shown in Figure 5. In this case, a solution containing 250 μM FcMeOH and PBS 1X is flowed through the device by gravity (as shown in Figure 4a). Figure 5a shows
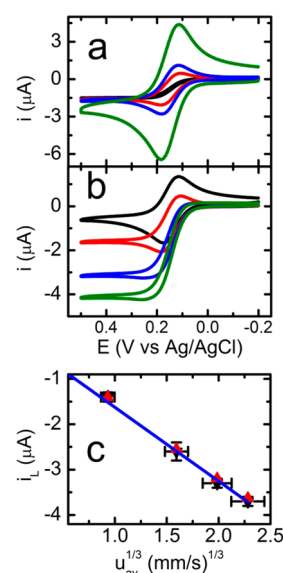

Figure 5. (a) CVs of 250 μM FcMeOH in PBS 1X as a function of scan rate. The black, red, blue, and green lines correspond to ν = 5, 50, 100, and 500 mV/s, respectively. The pressure drop within the HC was held constant at 0.3 mbar. R_{comp} = 7 kΩ; S_{WE} = 0.040 ± 0.004 cm^2. (b) CVs of 250 μM FcMeOH in PBS 1X as a function of the pressure in the HC. The black, red, blue, and green lines correspond to P = 0, 0.3, 1.5, and 2.9 mbar, respectively. ν = 50 mV/s; R_{comp} = 7 kΩ; S_{WE} = 0.040 ± 0.004 cm^2. (c) Experimental i_L (black triangles) plotted as a function of $(u_{av})^{1/3}$. The values of u_{av} were calculated using the experimentally determined value of P and the slope of the linear fit in Figure 4c. The vertical and horizontal error bars correspond to the standard deviation obtained using three independent devices and the standard deviation of the fit in Figure 4c, respectively. The blue line is a least-squares fit of the experimental data (slope = −1.63 ± 0.02 μA/(mm/s)$^{1/3}$; R^2 = 0.999). Values of i_L obtained by numerical simulation are plotted as red triangles. The parameters used for the simulations are provided in the Supporting Information. HC-PADs similar to the one presented in Figure 1a, that is, with the WE (carbon paste), CE (carbon paste), and RE (Ag/AgCl paste) positioned in the HC, were used to carry out the experiments shown in Figure 5.

CVs recorded as a function of ν at a constant pressure of 0.3 mbar. CVs recorded at a constant value of ν = 50 mV/s and different pressures are plotted in Figure 5b. When P increases and/or ν decreases, the shape of the CVs changes progressively from the shape observed in Figure 1b (characteristic of 1D semi-infinite diffusion) to a sigmoidal shape (characteristic of steady-state mass transfer).

The foregoing discussion indicates that the diffusion layer is affected by convection in a logical way. That is, when convection dominates, the current tends toward a constant, mass-transport-limited value, i_L.[35] Figure 5c shows the value of i_L, obtained at several different pressures, as a function of $(u_{av})^{1/3}$ (black triangles). Here the value of u_{av} was calculated using the value of P applied at the inlet of the device and the slope of the best-fit line in Figure 4c. The blue line in Figure 5c is a linear fit of the experimental data, and the red triangles, which are nearly superimposed on the experimental data, are the limiting currents calculated by numerical simulation. The linear variation of i_L with $(u_{av})^{1/3}$ corresponds to the "Levich" mass transfer regime.[42] Under these conditions, convection dominates diffusion and several approximations can be made to obtain an analytical relation (eq 4) between the steady-state limiting current and the linear flow rate.[35,42]

$$i_L = 0.925 \times n \times F \times w \times C° \times (l_e \times D)^{2/3}$$

$$\times \left(\frac{4 \times u_{av}}{h}\right)^{1/3} \tag{4}$$

Here, n is the equivalents of electrons, F is the Faraday constant, and $C°$ is the bulk concentration of the redox probe. From the slope of the linear fit (Figure 5c) and eq 4, the apparent height (h) of the channel was calculated to be 148 μm. This value reflects the height of the wetted channel, which, as discussed earlier in the context of Figure S3, is smaller than that of the dry channel ($\sim$170 μm).

The calculated channel height (148 μm) was used with the other experimental parameters to carry out a numerical simulation of convection and diffusion in an HC. The details of the simulation are provided in the Supporting Information. Briefly, however, the experimentally determined value of u_{av} (obtained from the fit in Figure 4c) and no-slip boundaries were used to solve the Navier–Stokes equation and hence obtain the flow profile in the HC. The concentration of FcMeOH at the electrode was set to zero (that is, the mass-transport-limited condition). Just a 1.5% difference is observed between the simulation and the experimental data. More importantly, the numerical simulation indicates that under our experimental conditions a Levich regime is expected, in agreement with the experimental result.

The agreement between the experimental data and the simulation is remarkable considering the roughness and hydrophobicity of both the walls and the electrodes,[43−46] as well as the swelling and mechanical deformation of the HC (see Supporting Information). This good agreement suggests that the approximations invoked for the simulations (the no-slip boundaries, perfectly smooth walls, perfectly orthogonal walls, no effects due to the hydrophobicity of the walls, and variable channel height) are reasonable. Numerical simulations and eq 4 can thus be used to accurately model electrochemistry in HC-PADs under convective conditions.

SUMMARY AND CONCLUSIONS

The key finding reported here is that HC-PADs provide reproducible, quantitative, and predictable electrochemical data. These are critical requirements for the development of reliable paper-based POC electrochemical sensors.[1] For example, in the absence of convection two different regimes are observed: one for short times (<15 s), representing 1D semi-infinite diffusion, and a second case (>15 s), where the diffusion layer extends through the entire height of the channel. In the presence of convection, the electrochemical data are reproducible and quantitatively exhibit Levich behavior.

Fast pressure-driven flow is one of the most seductive aspects of HC-PADs, because it leads to a shortened analysis time or enables sensors having longer channels.[22] Flow can be initiated using just a drop of fluid, and under the conditions described here flow is laminar and the average linear flow rate varies linearly with P from 0.8 to 12 mm/s. Interestingly the flows in HC-PADs and plastic-based devices are similar despite the nonidealities (especially mechanical deformations in the wet state) of HC-PADs. This finding opens the possibility of implementing strategies that are already well developed for plastic and glass platforms, but at a much lower cost.

Our present studies are directed toward the design, fabrication, and testing of a new family of electrochemical sensors based on HC-PADs. This new generation of PADs will incorporate additional functionalities, including our recently reported SlipPAD concept,[10] that provide enhanced capabilities while adding just minimal additional complexity. The results of these studies will be reported in due course.

ASSOCIATED CONTENT

S **Supporting Information**

Patterns of the paper devices, cross-sectional micrographs of dry and wet HCs, Randles–Sevcik and Cottrell equations, CAs corresponding to a 15 min experiment, calculation of the Reynolds number, collection efficiencies and time delays at various pressures, generation–collection experiments in paper-channel PADs, measurement of the volumetric flow rate, and details regarding the numerical simulations. This material is available free of charge via the Internet at http://pubs.acs.org.

AUTHOR INFORMATION

Corresponding Author

crooks@cm.utexas.edu

Notes

The authors declare no competing financial interest.

ACKNOWLEDGMENTS

REFERENCES

(1) Maxwell, J. E.; Mazzeo, A. D.; Whitesides, G. M. *MRS Bull.* **2013**, *38*, 309.

(2) Martinez, A. W.; Phillips, S. T.; Butte, M. J.; Whitesides, G. M. *Angew. Chem., Int. Ed.* **2007**, *46*, 1318.

(3) Martinez, A. W.; Phillips, S. T.; Whitesides, G. M. *Proc. Natl. Acad. Sci. U.S.A.* **2008**, *105*, 19606.

(4) Carrilho, E.; Phillips, S. T.; Vella, S. J.; Martinez, A. W.; Whitesides, G. M. *Anal. Chem.* **2009**, *81*, 5990.

(5) Martinez, A. W.; Phillips, S. T.; Whitesides, G. M.; Carrilho, E. *Anal. Chem.* **2010**, *82*, 3.

(6) Cheng, C.-M.; Martinez, A. W.; Gong, J.; Mace, C. R.; Phillips, S. T.; Carrilho, E.; Mirica, K. A.; Whitesides, G. M. *Angew. Chem., Int. Ed.* **2010**, *49*, 4771.

(7) Delaney, J. L.; Hogan, C. F.; Tian, J.; Shen, W. *Anal. Chem.* **2011**, *83*, 1300.

(8) Yu, J.; Ge, L.; Huang, J.; Wang, S.; Ge, S. *Lab Chip* **2011**, *11*, 1286.

(9) Yang, X.; Forouzan, O.; Brown, T. P.; Shevkoplyas, S. S. *Lab Chip* **2012**, *12*, 274.

(10) Liu, H.; Li, X.; Crooks, R. M. *Anal. Chem.* **2013**, *85*, 4263.

(11) Liu, H.; Xiang, Y.; Lu, Y.; Crooks, R. M. *Angew. Chem., Int. Ed.* **2012**, *51*, 6925.

(12) Yetisen, A. K.; Akram, M. S.; Lowe, C. R. *Lab Chip* **2013**, *13*, 2210.

(13) Nery, E. W.; Kubota, L. T. *Anal. Bioanal. Chem.* **2013**, *405*, 7573.

(14) Parolo, C.; Merkoci, A. *Chem. Soc. Rev.* **2013**, *42*, 450.

(15) Lewis, G. G.; DiTucci, M. J.; Phillips, S. T. *Angew. Chem., Int. Ed.* **2012**, *51*, 12707.

(16) Liu, H.; Crooks, R. M. *J. Am. Chem. Soc.* **2011**, *133*, 17564.

(17) Fu, E.; Lutz, B.; Kauffman, P.; Yager, P. *Lab Chip* **2010**, *10*, 918.

(18) Osborn, J. L.; Lutz, B.; Fu, E.; Kauffman, P.; Stevens, D. Y.; Yager, P. *Lab Chip* **2010**, *10*, 2659.

(19) Lutz, B. R.; Trinh, P.; Ball, C.; Fu, E.; Yager, P. *Lab Chip* **2011**, *11*, 4274.

(20) Apilux, A.; Ukita, Y.; Chikae, M.; Chailapakul, O.; Takamura, Y. *Lab Chip* **2013**, *13*, 126.

(21) Glavan, A. C.; Martinez, R. V.; Maxwell, E. J.; Subramaniam, A. B.; Nunes, R. M. D.; Soh, S.; Whitesides, G. M. *Lab Chip* **2013**, *13*, 2922.

(22) Renault, C.; Li, X.; Fosdick, S. E.; Crooks, R. M. *Anal. Chem.* **2013**, *85*, 7976.

(23) Dungchai, W.; Chailapakul, O.; Henry, C. S. *Anal. Chem.* **2009**, *81*, 5821.

(24) Nie, Z.; Nijhuis, C. A.; Gong, J.; Chen, X.; Kumachev, A.; Martinez, A. W.; Narovlyansky, M.; Whitesides, G. M. *Lab Chip* **2010**, *10*, 477.

(25) Nie, Z.; Deiss, F.; Liu, X.; Akbulut, O.; Whitesides, G. M. *Lab Chip* **2010**, *10*, 3163.

(26) Carvalhal, R. F.; Simão Kfouri, M.; de Oliveira Piazzetta, M. H.; Gobbi, A. L.; Kubota, L. T. *Anal. Chem.* **2010**, *82*, 1162.

(27) Thom, N. K.; Yeung, K.; Pillion, M. B.; Phillips, S. T. *Lab Chip* **2012**, *12*, 1768.

(28) Liu, H.; Crooks, R. M. *Anal. Chem.* **2012**, *84*, 2528.

(29) Wang, P.; Ge, L.; Yan, M.; Song, X.; Ge, S.; Yu, J. *Biosens. Bioelectron.* **2012**, *32*, 238.

(30) Bard, A. J.; Faulkner, L. R. *Electrochemical methods: fundamentals and applications*, 2nd ed.; Wiley & Sons: New York, 2000.

(31) Anicet, N.; Bourdillon, C.; Moiroux, J.; Savéant, J.-M. *J. Phys. Chem. B* **1998**, *102*, 9844.

(32) Laschi, S.; Palchetti, I.; Marrazza, G.; Mascini, M. *J. Electroanal. Chem.* **2006**, *593*, 211.

(33) Wang, J.; Tian, B.; Nascimento, V. B.; Angnes, L. *Electrochim. Acta* **1998**, *43*, 3459.

(34) Fanjul-Bolado, P.; Hernández-Santos, D.; Lamas-Ardisana, P. J.; Martín-Pernía, A.; Costa-García, A. *Electrochim. Acta* **2008**, *53*, 3635.

(35) Amatore, C.; Da Mota, N.; Sella, C.; Thouin, L. *Anal. Chem.* **2007**, *79*, 8502.

(36) Kenis, P. J. A.; Ismagilov, R. F.; Takayama, S.; Whitesides, G. M.; Li, S.; White, H. S. *Acc. Chem. Res.* **2000**, *33*, 841.

(37) Seong, G. H.; Crooks, R. M. *J. Am. Chem. Soc.* **2002**, *124*, 13360.

(38) Gad-el-Hak, M., Ed. *MEMS: Introduction & Fundamentals*; CRC Press: Boca Raton, FL, 2005.

(39) Licht, S.; Cammarata, V.; Wrighton, M. S. *Science* **1989**, *243*, 1176.

(40) Amatore, C.; Belotti, M.; Chen, Y.; Roy, E.; Sella, C.; Thouin, L. *J. Electroanal. Chem.* **2004**, *573*, 333.

(41) Compton, R. G.; Stearn, G. M. *J. Chem. Soc., Faraday Trans. 1* **1988**, *84*, 4359.

(42) Levich, V. G. *Physicochemical Hydrodynamics*; Prentice-Hall, Inc.: Engelwood Cliffs, NY, 1962.

(43) Bahrami, M.; Yovanovich, M. M.; Culham, J. R. *J. Fluids Eng.* **2005**, *128*, 632.

(44) Zhi-Xin, L.; Dong-Xing, D.; Zeng-Yuan, G. *Microscale Therm. Eng.* **2003**, *7*, 253.

(45) Phares, D. J.; Smedley, G. T. *Phys. Fluids* **2004**, *16*, 1267.

(46) Niavarani, A.; Priezjev, N. V. *Phys. Fluids* **2009**, *21*, 052105.